Neutralization–Reionization of alkenylammonium cations: An experimental and ab initio study of intramolecular N–H … C=C interactions in cations and hypervalent ammonium radicals

ARTICLE *in* JOURNAL OF THE AMERICAN SOCIETY FOR MASS SPECTROMETRY · NOVEMBER 1997

Impact Factor: 2.95 · DOI: 10.1016/S1044-0305(97)00184-0

3 AUTHORS, INCLUDING:

Scott A Shaffer
University of Massachusetts Medical School
82 PUBLICATIONS **2,684** CITATIONS
SEE PROFILE

František Tureček
University of Washington Seattle
166 PUBLICATIONS **2,496** CITATIONS
SEE PROFILE

Neutralization–Reionization of Alkenylammonium Cations: An Experimental and Ab Initio Study of Intramolecular N–H · · · C=C Interactions in Cations and Hypervalent Ammonium Radicals

Scott A. Shaffer,* Jill K. Wolken, and František Tureček
Department of Chemistry, Bagley Hall, University of Washington, Seattle, Washington, USA

A series of isomeric hexenylammonium and hexenyldimethylammonium cations were neutralized by collisional electron transfer in the gas phase in an attempt to generate hypervalent ammonium radicals. The radicals dissociated completely on the 4.8–5.4 μs time scale. Radicals in which the hexene double bond was in the 3-, 4-, and 5-positions dissociated by competitive N–H and N–C bond cleavages. Allylic 2-hexen-1-ylammonium and 2-hexen-1-yldimethylammonium radicals underwent predominant cleavages of allylic N–C bonds. Deuterium labeling experiments revealed no intramolecular hydrogen transfer from the hypervalent ammonium group to the hexene double bond. Ab initio and density functional theory calculations showed that alkenylammonium and alkenylmethyloxonium ions preferred hydrogen bonded structures in the gas phase. The stabilization through intramolecular H bonding in 3-buten-1-ylammonium and 3-buten-1-yl methyloxonium ions was calculated by B3LYP/6-311G(2d,p) at 26 and 18 kJ mol^{-1}, respectively. No intramolecular hydrogen bonding was found for the allylammonium ion. The hypervalent 3-buten-1-yl-methyloxonium radical was calculated to be unbound and predicted to dissociate exothermically by O–H bond cleavage. This dissociation may provide kinetic energy for the hydrogen atom to overcome a small energy barrier for exothermic addition to the double bond. The 3-buten-1-ylammonium and allylammonium radicals were found to be bound and preferred gauche conformations without intramolecular hydrogen bonding. Vertical neutralization of alkenylammonium ions was accompanied by small Franck–Condon effects. The failure to detect stable or metastable hypervalent alkenylammonium radicals was ascribed to the low activation barriers to exothermic dissociations by N–H and N–C bond cleavages. (J Am Soc Mass Spectrom 1997, 8, 1111–1123) © 1997 American Society for Mass Spectrometry

Collisional neutralization of gaseous even-electron cations deposits an electron in one of the unoccupied molecular orbitals to produce radicals in their ground or excited electronic states. For a carbocation or an unsaturated heteroatom-centered cation, the radical formed is often bound and can be detected as a stable species using neutralization–reionization mass spectrometry (NRMS) [1–4]. For a saturated onium cation (onium refers to ammonium, oxonium, sulfonium, etc.), the radical formed by neutralization represents a hypervalent species [5, 6] that is often unbound or weakly bound in the ground electronic state [7–15].

Address correspondence to Dr. František Tureček, Department of Chemistry, Bagley Hall, Box 351700, University of Washington, Seattle, WA 98195-1700. E-mail: turecek@macmail.chem.washington.edu

* Current address: Pacific Northwest National Laboratory, Richland, WA 99352.

Stabilization in hypervalent radicals due to the presence of another functional group has been reported for a few systems. For example, phenyl groups bearing electronegative substituents can stabilize the neutralized species by capturing the incoming electron to form a metastable zwitterion [16]. Hydrogen bonding was reported to stabilize ammonium radicals in $NH_4^{\bullet}NH_3$ clusters [17, 18], whereas intramolecular H bonding in ammonium ions derived from organic diamines did not result in stabilization of hypervalent radicals following collisional electron transfer [13]. The existence of Rydberg molecules, e.g., $NH_4^{\bullet}{\cdot}NH_4$ in which the odd electrons pair to form a weak bond, has been a matter of recent argument [19, 20].

We have reported recently on the unusual behavior of hypervalent oxonium radicals derived from protonated methoxyhexenes [21]. In those systems, the hydrogen atom residing on the hypervalent oxygen atom

Published by Elsevier Science Inc.
1044-0305/97/$17.00
PII S1044-0305(97)00184-0

Received May 5, 1997
Revised July 18, 1997
Accepted July 21, 1997

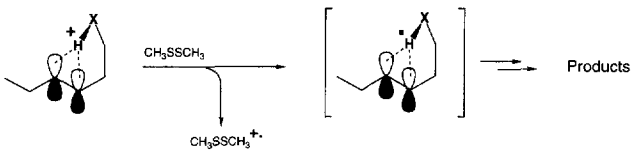

Scheme I

was transferred intramolecularly onto the hexene double bond, as distinguished by specific deuterium labeling. We argued that since a rearrangement by hydrogen transfer is typically slower than a direct bond cleavage [22], the slow reaction may provide a clock for the estimation of the lifetime of the hypervalent radical intermediate. Such a radical clock [23] may potentially be used to detect transient intermediates on a time scale that is much shorter than the usual 10^{-7}–10^{-6} s amenable to NRMS measurements [1–4]. The present work reports a study of hypervalent ammonium radicals derived from protonated hexenamines **1–4** and N,N-dimethylaminohexenes **5–8**. These systems offer two distinct structural features. First, the primary and tertiary amino groups are far more basic than the hexene double bond, as judged from the proton affinities of related alkenes and aliphatic amines [24–26]. Thus, a gas-phase acid can be chosen such as to protonate hexenamines selectively at the amine nitrogen. Second, the position of the double bond with respect to the protonated amino group can be varied from 5-hexenyl, as in **1** and **5**, through 2-hexenyl, as in **4** and **8**. This allows one to investigate structure effects on hydrogen bonding between the double-bond pi system and the ammonium proton(s) in the cations and hypervalent ammonium radicals. We also investigate by density functional theory calculations [27] the hydrogen bonding in model alkenylammonium and alkenyl-methyloxonium cations and hypervalent radicals formed by vertical electron transfer (Scheme I, $X = NH_2$ and OCH_3). We address the question of whether an intramolecular interaction between the ammonium group and the double bond in the hypervalent radical can result in (i) stabilization, (ii) hydrogen transfer followed by formation of a stable carbon-centered radical intermediate, or (iii) opening of a distinct dissociation pathway.

Experimental

Methods

Neutralization–reionization mass spectra were obtained on a tandem quadrupole acceleration–deceleration mass spectrometer, as described previously [28]. Ammonium cations were generated by ammonia chemical ionization (CI) in a tight ion source at 180–200 °C and at reagent gas pressures ensuring efficient protonation and minimizing the formation of amine cation radicals. This precaution was important in order to prevent contamination of the $(M + H)^+$ ions with the ^{13}C isotope satellites of $M^{+\cdot}$ at the same nominal mass-to-change ratio values. The optimized ammonia pressure in the ion source was estimated at 0.1–0.2 Torr. The $[M + H]^+/[M^{+\cdot}]$ ratios for the hexenamines were >20 in most instances. Gas-phase deuteronations were conducted with ND_3–CI (ND_3, Matheson, 99% D). The cations were accelerated to 8200 eV kinetic energy and neutralized by collisions with gaseous dimethyldisulfide at pressures allowing 70% transmittance of the precursor ammonium ion beam. The residual ions were reflected by a special cylindrical lens, and the neutral intermediates were reionized to cations by collisions with oxygen in a downbeam collision cell. The oxygen pressure was adjusted to achieve 70% transmittance of the precursor ion beam. Neutral lifetimes corresponding to the drift time between the neutralization and reionization cells were 4.8 and 5.4 μs for **1a**$^{\cdot}$–**4a**$^{\cdot}$ and **5a**–**8a**$^{\cdot}$, respectively.

Collision-induced dissociation (CID) spectra were obtained on a Kratos Profile HV-4 double focusing sector mass spectrometer of forward (electrostatic sector *E* precedes magnet *B*) geometry. 4-keV ions were dissociated in a grounded collision cell mounted in the first-field free region. The product ions were analyzed by a linked scan of *E* and *B*, keeping the *B*/*E* ratio constant. Oxygen was used as a collision gas that was admitted to the collision cell at pressures allowing 70% transmittance of the precursor ion beam. The CID spectra were averaged over 20–40 repetitive scans. Electron-impact mass spectra were also obtained on the Kratos Profile HV-4 instrument. The samples were introduced in the ion source from a glass liquid introduction system at room temperature.

Materials

Hexenamines **1–3** were prepared from the corresponding bromohexenes by standard azide syntheses (excess NaN_3, dimethylsulfoxide, 20 °C overnight), followed by reduction of the hexenylazides with lithium aluminum hydride in refluxing ether [29]. 2-Hexen-1-amine **(4)** was synthesized by the Overman trichloroacetimidate method [30]. N,N-dimethylamino-hexenes **5–8** were synthesized by reacting the corresponding bromohexenes with a large excess of dimethylamine [29]. The products were purified by short-path distillation and characterized by ^1H-NMR spectra and gas-chromatography mass spectrometry. The supporting spectroscopic data are available from the corresponding author upon request.

Calculations

Standard ab initio calculations were conducted using the GAUSSIAN 94 suite of programs [31]. The geometries of model amine and ether cations were optimized with spin-restricted Hartree–Fock calculations (RHF) using the 6-31G(d) basis set. Harmonic frequencies were obtained at the same level of theory and, after scaling by 0.893 [32], used to obtain zero-point energy corrections.

Enthalpies, entropies, and free energies were obtained from standard thermodynamic equations using the calculated moments of inertia and scaled harmonic frequencies. Improved energies including electron correlation effects were obtained by single point calculations using the Moller–Plesset perturbation theory [33] truncated at second order (MP2) with frozen core excitations [32]. The single-point calculations were carried out with the larger 6-311G(2d,p) basis set [34] that was shown recently to give excellent proton affinities for a series of amines [35–38]. Alternatively, density functional theory calculations were employed to obtain optimized geometries and energies using Becke's hybrid functional (B3LYP) [39] and the 6-311G(2d,p) or 6-31G(d,p) basis sets. Calculations on hypervalent ammonium and oxonium radicals were performed with B3LYP/6-31++G(d,p) to take into account both the effects of electron correlation and the diffuse character of molecular orbitals in hypervalent onium species [7, 11].

Results and Discussion

Hexenylammonium Ions

Cations $\mathbf{1a}^+$–$\mathbf{4a}^+$ are the precursors of hypervalent hexenylammonium radicals of interest. The properties of these ammonium cations were therefore investigated first through their CID spectra (Table 1). The CID spectra of ions $\mathbf{1a}^+$–$\mathbf{4a}^+$ showed loss of ammonia to produce $C_6H_{11}^+$ ions at *m/z* 83, which underwent further dissociations to yield hydrocarbon ions at *m/z* 67, 55, 41, and 39 (Table 1). In addition, nitrogen-containing ions were formed that appeared at *m/z* 30 ($CH_2NH_2^+$), 31 ($^+CH_2NH_3^+$), 44, 45, 56, and 70. The relative abundances of the CID fragment ions depended on the position of the double bond (Table 1).

Deuterium labeling was used to determine the interaction of the ammonium and hexenyl groups in dissociating ions. CID of $\mathbf{1b}^+$ showed formation of $C_6H_{11}^+$, $C_6H_{10}D^+$, and $C_6H_9D_2^+$ in a 22:6:1 ratio. This indicated a limited H/D exchange between the ammonium group and the 5-hexenyl chain preceding or accompanying the elimination of ammonia. However, the fragments originating by consecutive dissociations of the $[MD - N(H,D)_3]^+$ ions showed a low deuterium content, viz., the [*m/z* 68]/[*m/z* 67] and [*m/z* 56]/[*m/z* 55] ratios in Table 1. The eliminations of C_2H_6 (*m/z* 70 and 73), C_3H_8 (*m/z* 56 and 58), and the formations of $CH_2NH_3^{+\bullet}$ and $CH_2NH_2^+$ showed clean mass shifts on deuteration, which indicated negligible H/D exchange between the ammonium and 5-hexenyl groups. CID of $\mathbf{2b}^+$ revealed the formation of $C_6H_{11}^+$ by loss of ND_3 and $C_6H_{10}D^+$ by loss of ND_2H in a 4.4:1 ratio. Exchange between the ammonium group and the 4-hexenyl group thus occurred to some extent during the elimination of ammonia. However, the products of subsequent fragmentations of $C_6H_{11}^+$ showed negligible deuterium content, viz., the [*m/z* 68]/[*m/z* 67] and [*m/z* 56]/[*m/z* 55] ratios in Table 1. These apparently contradictory results can be interpreted as follows. Direct elimination of ND_3 from $\mathbf{1b}^+$ and $\mathbf{2b}^+$ formed a reactive $C_6H_{11}^+$ isomer that dissociated extensively to form unlabeled hydrocarbon ions. Isomerization in $\mathbf{1b}^+$ and $\mathbf{2b}^+$ by H/D exchange followed by elimination of ND_2H formed a more stable hexenyl ion that dissociated less and thus gave rise to the observed $[C_6H_{11}]^+/[C_6H_{10}D]^+$ ratio. Elimination of C_3H_8 and the formation of $CH_2ND_2^+$ and $^+CH_2ND_3^+$ proceeded cleanly with no significant H/D exchange.

The ND_3-labeled ion $\mathbf{3b}^+$ showed a clean elimination of ND_3 and a mass shift of *m/z* 30 to *m/z* 32 for $CH_2ND_2^+$. Hydrogen/deuterium exchange between the ammonium group and the 3-hexenyl chain was negligible. CID of $\mathbf{4b}^+$ showed a clean elimination of ND_3 to form $C_6H_{11}^+$ at *m/z* 83, and a predominant formation of ND_3H^+ (Table 1). Mass shifts due to the presence of deuterium were observed for *m/z* 71 to *m/z* 74, *m/z* 56 to *m/z* 58, 59, *m/z* 31 to *m/z* 34, and *m/z* 30 to *m/z* 32. These mass shifts and the absence thereof for the $C_6H_{11}^+$ ion were consistent with the retention of deuterium in the ammonium or amine group. In particular, they indicated negligible proton/deuteron exchange between the ammonium group and the 2-hexenyl chain prior to or during the loss of ammonia. The elimination of C_3H_8 and the formation of $CH_2NH_2^+$ occurred with a hydrogen transfer from the ammonium group. However, the labeling showed negligible *reverse* transfer that would have resulted in H/D scrambling in the ions formed.

To summarize, the dissociations of $\mathbf{1a}^+$–$\mathbf{4a}^+$ proceeded by loss of ammonia and cleavages of the hexenyl chain. The neutral fragments formed by these dissociations were NH_3, C_2H_{4-6}, C_3H_{6-8}, and C_4H_7. Negligible proton exchange between the ammonium and hexenyl groups was found for dissociating $\mathbf{3a}^+$ and $\mathbf{4a}^+$, whereas limited exchange was found for $\mathbf{1a}^+$ and $\mathbf{2a}^+$.

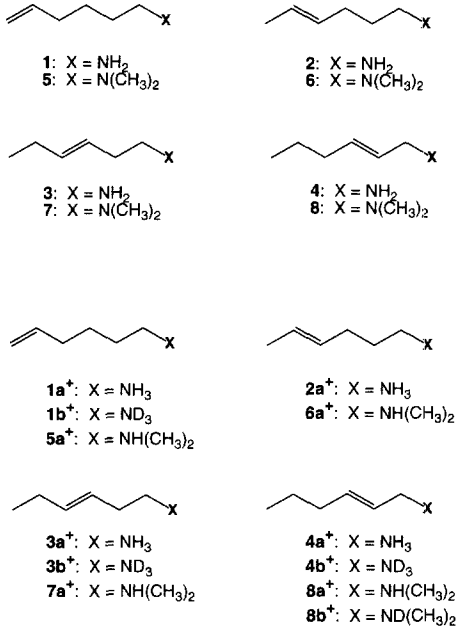

Table 1. Collision-induced dissociation spectra of $1a^+$–$4b^+$

	Relative intensity[a]							
m/z	$1a^+$	$1b^+$	$2a^+$	$2b^+$	$3a^+$	$3b^+$	$4a^+$	$4b^+$
15	0.7	2	0.2					0.4
17	3.5		2.2		0.9		1	
18	35		17		6.1		20	
19		1					0.2	
20		17		12		5.3		
21		68		38		17		54
22		1.5			4	0.8		0.3
26	4.4	4.6	2.7	1.2	1.5	1.4	1.6	1.1
27	24	35	20	27	10	13	13	13
28	17	11	13	9.3	6.2	4.5	7.6	3.5
29	16	16	15	21	7	10	7	6.5
30	100	4.2	88	6.5	52	1.5	11	0.8
31	8.5	9.4	5.8	3.5	3.4	1.4	2.5	0.6
32		69		91		48		4.7
33		4.9		1.1		1.8		1.4
34		13		7.5		3.8		2.4
37	0.2	2.2	0.4		0.5			0.7
38	3.7	3.8	2.6	0.7	1.8	0.9	2	
39	43	45	35	37	17	17	20	18
40	6.9	9.6	5	5.4	3.5	3.7	3.3	1.7
41	80	85	41	46	31	28	35	38
42	14	10	10	9	5	5	4	2
43	13	5	13	5	4.5	3	5	3.5
44	10	3.3	14	3	1.3	2	0.5	0.8
45	14	7	12	7	2.5	1.6		0.6
46		3		7		2.2		
47		9.5		11		0.7		
48		15		13		3.3		
50	2.4	3.4	3	0.5	2.4	1	2.1	1
51	3.4	5.4	3.2	3.3	2.7	2.4	3.1	3
52	2.8	2.8	2.8	1.6	2.3	2	3.3	2.1
53	15	13	14	14	9	9	10	4.8
54	19	25	13	13	7	6	26	26
55	93	100	100	100	43	36	42	30
56	38	6.5	20	7.7	4.4	2.3	20	1.7
57	3.2	2.9	2.2		0.2		1.1	0.6
58	5.4	33	0.4	11	0.2	2.4		5.3
59	1.8	4.2	1.2	1.6		0.8		3.4
60								1.1
61		6.8						
62		3.2						
65	2	2.4	2.3		2.4	1.7	2.4	1.4
66	2	2.5	2.1	0.6	2.1	1.2	2.2	1.3
67	20	23	23	21	20	12	14	12
68	1.4	1.6	3.2	2.7	4.8	3.5	4.5	3.2
69	1	0.4	0.5		2.4	1.3	2.4	
70	6		3		1		6.7	
71			0.3				6.2	1
72		0.8						1
73	1.1	4.3						3
74								5.5
76		2						
77	1.7	2	1.3		1.2	1	1.2	0.5
79	5	4.6	3.3	1.6	3	2.3	3.2	2.5
80	1.5	2	1		1	0.5	1.2	0.6
81	5.4	4.2	4.5	1.8	3.5	2	3.3	1.7
82	9	4.3	23	19	25	14	12	9
83	39	31	36	53	100	100	100	100
84	4	8	2	12	3	5	3	8
85		1.4			0.4			
98	1.2		0.8		0.5		1.1	
99	(14)[b]		(13)[b]		(3)[b]		(4)[b]	

(Continued)

Table 1. Collision-induced dissociation spectra of $1a^+$–$4b^+$ *(continued)*

	Relative intensity[a]							
m/z	$1a^+$	$1b^+$	$2a^+$	$2b^+$	$3a^+$	$3b^+$	$4a^+$	$4b^+$
100	–[c]		–[c]		–[c]		–[c]	0.7
101		0.7				0.4		0.4
102		(12)[b]		(2)[b]		(7)[b]		(21)[b]
103		–[c]		–[c]		–[c]		–[c]

[a] Percent of the most abundant fragment ion.
[b] Relative intensities of ions at *m/z* adjacent to those of the precursors may be affected by artifacts in *B/E* linked scans.
[c] Precursor ion intensities omitted.

Hexenylammonium Radicals

Neutralization with dimethyldisulfide of $1a^+$–$4a^+$ followed by reionization with oxygen resulted in *complete dissociation*, such that no survivor ions $1a^+$–$4a^+$ were detected in the NR spectra (Figure 1). Hence, the intermediate hypervalent radicals **1a**•–**4a**• were unstable on the 4.8-μs time scale of these measurements. The NR spectra showed weak peaks of NH_3 and hydrocarbon fragments of the C_6H_{5-10} group at *m/z* 77–82, C_5H_7 at *m/z* 67, C_4H_{2-7} at *m/z* 50–55, C_3H_{3-7} at *m/z* 39–43, and C_2H_{1-5} at *m/z* 25–29. The relative intensities of the hydrocarbon fragments differed for $1a^+$–$4a^+$. Nitrogen-containing fragments were found at *m/z* 56 (loss of C_3H_8) and *m/z* 30 (CH_2NH_2).

In order to elucidate the dissociations of **1a**•–**4a**•, the neutral products must be identified through signature peaks in their mass spectra [16]. The anticipated neutral products were amines **1**–**4**, ammonia, and C_6H_{11}• radicals. Cation radicals $1^{+\bullet}$–$4^{+\bullet}$ were found to dissociate extensively when formed by 70-eV electron impact ionization of amines **1**–**4**, which gave very weak molecular ions. The ion dissociations produced fragments at *m/z* 82 (M − NH_3, $C_6H_{10}^{+\bullet}$), 70 (M − C_2H_6, $C_4H_8N^+$), 67 ($C_5H_7^+$), 56 (M − C_3H_8, $C_3H_6N^+$), and 30 ($CH_2NH_2^+$) that were representative of amines **1**–**4**. To characterize the C_6H_{11}• fragment from **4a**•, the $CH_3CH_2CH_2CH$–$CH{=}CH_2^+$ allylic ion was generated by loss of methanol from protonated 1-methoxyhex-2-ene [21], and its NR spectrum was obtained for reference. The spectrum (Figure 2) displayed a $C_6H_{11}^+$ survivor ion, and major hydrocarbon fragments of the C_6H_{5-10}, C_5H_{5-8}, C_4H_{3-7}, C_3H_{3-6}, and C_2H_{1-5} groups. Other C_6H_{11}• primary radicals could possibly be formed by dissociations of **1a**•–**3a**•. However, the corresponding $C_6H_{11}^+$ ions were not available for reference, and their preparation and characterization was likely to be difficult because of the

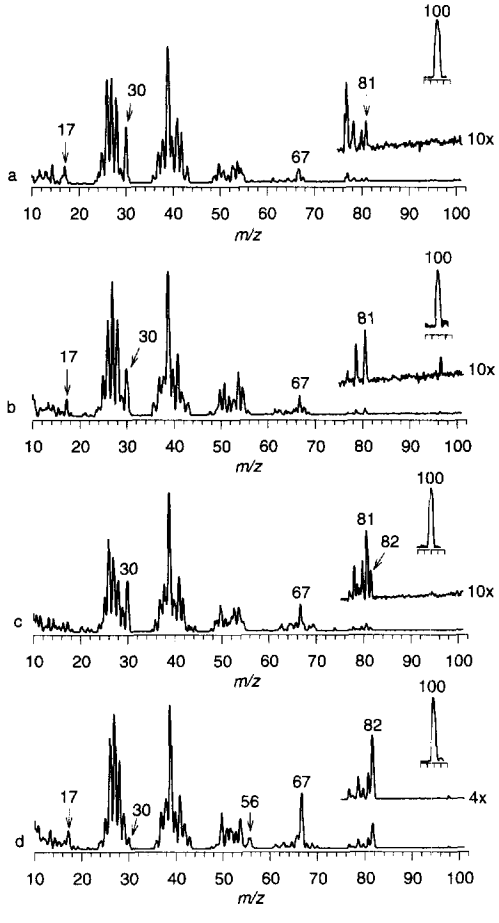

Figure 1. Neutralization–reionization (CH_3SSCH_3, 70% transmittance/O_2, 70% transmittance) mass spectra of (**a**) $1a^+$, (**b**) $2a^+$, (**c**) $3a^+$, and (**d**) $4a^+$. Insets show the $(M + H)^+$ regions in the CI mass spectra.

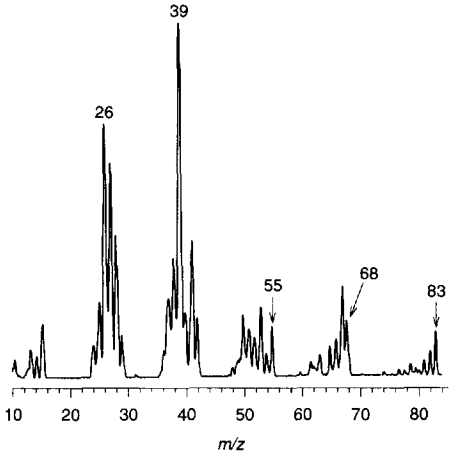

Figure 2. Neutralization–reionization mass spectrum of $C_6H_{11}^+$ from protonation of 1-methoxyhex-2-ene. The collision conditions were as in Figure 1.

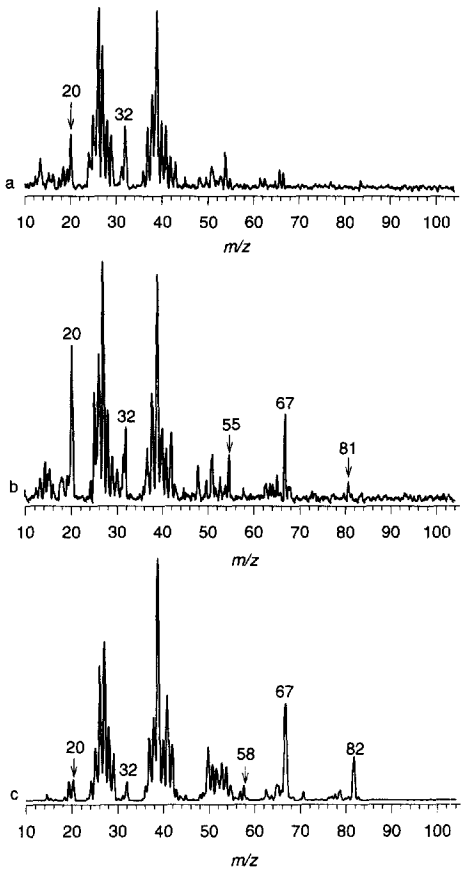

Figure 3. Neutralization–reionization mass spectra of (a) $\mathbf{1b}^+$, (b) $\mathbf{3b}^+$, (c) $\mathbf{4b}^+$. The collision conditions were as in Figure 1.

instability of primary alkenyl carbocations and their tendency to isomerize to allylic structures [40].

The fragments in the NR spectra of $\mathbf{1a}^+$–$\mathbf{4a}^+$ pointed to two major dissociations of **1a**–**4a**. First, loss of H$^\bullet$ by N–H bond cleavage formed amines **1**–**4**, which dissociated following ionization. The $CH_2NH_2^+$ ion that was present in the NR spectra of $\mathbf{1a}^+$–$\mathbf{4a}^+$ was a signature for the formation of **1**–**4**. Second, cleavage of the N–C bond in $\mathbf{1a}^\bullet$–$\mathbf{4a}^\bullet$ gave rise to ammonia and $C_6H_{11}^\bullet$, as documented by the small peaks of reionized $NH_3^{+\bullet}$ that appeared in the NR spectra of $\mathbf{1a}^+$–$\mathbf{4a}^+$ (Figure 1). Ions due to reionization of the complementary $C_6H_{11}^\bullet$ radicals were undetectable (*m/z* 83), although the $C_6H_{10}^{+\bullet}$ (*m/z* 82) and $C_6H_9^+$ (*m/z* 81) dehydrogenation products appeared in the NR spectra (Figure 1). The presence of abundant hydrocarbon fragments clearly indicated loss of ammonia from $\mathbf{1a}^\bullet$–$\mathbf{4a}^\bullet$. The absence of $C_6H_{11}^+$ in the NR spectra indicated facile dissociations of the intermediate $C_6H_{11}^\bullet$ radicals, reionized $C_6H_{11}^+$, or a combination of both processes.

The interaction between the ammonium and hexenyl groups in hypervalent hexenylammonium radicals was investigated for the labeled species $\mathbf{1b}^\bullet$, $\mathbf{3b}^\bullet$, and $\mathbf{4b}^\bullet$ (Figure 3). The NR spectra of $\mathbf{1b}^+$, $\mathbf{3b}^+$, and $\mathbf{4b}^+$ showed no detectable survivor ions at *m/z* 103, indicating no stabilization of hypervalent hexenylammonium radicals through deuterium isotope effects. The NR spectrum of $\mathbf{4b}^+$ showed no significant mass shifts for the hydrocarbon fragments at *m/z* 82, 67, and fragments of the C_4H_{1-7} and C_3H_{3-6} groups. A clean mass shift to *m/z* 32 was observed for $CH_2ND_2^+$. The peak of ammonia was split to $ND_3^{+\bullet}$ and $ND_2H^{+\bullet}$. The former ion was due to reionization of ND_3 from dissociation of $\mathbf{4b}^\bullet$. Alternatively, CAD of $\mathbf{4b}^+$ concurrent with collisional neutralization could produce a fraction of ND_3 that would yield $ND_3^{+\bullet}$ upon reionization. The formation of the $ND_2H^{+\bullet}$ ion could be interpreted in two ways. First, loss of D from $\mathbf{4b}^\bullet$ would form **1**-ND_2, which could eliminate NHD_2 to give rise to $ND_2H^{+\bullet}$ after reionization. Second, a H/D exchange in $\mathbf{4b}^\bullet$ followed by elimination of NHD_2 would also yield $ND_2H^{+\bullet}$ after reionization. However, the latter mechanism should also produce deuterium-containing hydrocarbon fragments, which were not observed. The NR spectra thus showed no significant interaction between the ammonium and 2-hexenyl groups in hypervalent radical $\mathbf{4a}^\bullet$ that would have resulted in hydrogen exchange.

The NR spectra of $\mathbf{1b}^+$ and $\mathbf{3b}^+$ were somewhat less informative because of the poorer signal-to-noise ratios achieved (Figure 3). Nevertheless, the hydrocarbon fragments showed no significant mass shifts due to the presence of deuterium. The peak of $ND_3^{+\bullet}$ showed no accompanying $ND_xH_{3-x}^{+\bullet}$ ions that would suggest H/D exchange in $\mathbf{3a}^\bullet$. Likewise, the NR spectrum of $\mathbf{1b}^\bullet$ displayed a clean peak of $ND_3^{+\bullet}$ and no significant mass shifts for the hydrocarbon fragments. The labeling data allowed us to conclude that the ammonium and hexenyl groups in $\mathbf{1a}^\bullet$ and $\mathbf{3a}^\bullet$ did not interact by intramolecular hydrogen transfer.

Ab Initio and Density Functional Theory Studies of Model Systems

The dissociations of hexenylammonium radicals $\mathbf{1a}^\bullet$–**4a** differed substantially from those of the analogous hexenylmethyloxonium radicals, in which extensive migration of the ether proton onto the hexenyl group was observed [21]. To gain more insight into these processes, we investigated the XH · · · C=C intramolecular interactions (X = NH_2, OCH_3) by ab initio calculations with model 3-buten-1-ylammonium and 3-buten-1-ylmethyloxonium ions and radicals. The 3-butenyl group allows for intramolecular hydrogen bonding through five- or six-membered cyclic structures and at the same time is small enough to permit ab initio calculations with reasonably large basis sets to treat the cations and radicals adequately. Optimized structures were obtained with B3LYP/6-311G(2d,p) for hydrogen-bonded and stretched 3-buten-1-ylammonium cations $\mathbf{9a}^+$ and $\mathbf{9b}^+$ (Figure 4) and 3-buten-1-yl methyloxonium cations $\mathbf{10a}^+$ and $\mathbf{10b}^+$ (Figure 5). Complete optimized parameters including bond and dihedral angles are available from the corresponding author on request.

Compared with the stretched rotamer $\mathbf{9b}^+$, the opti-

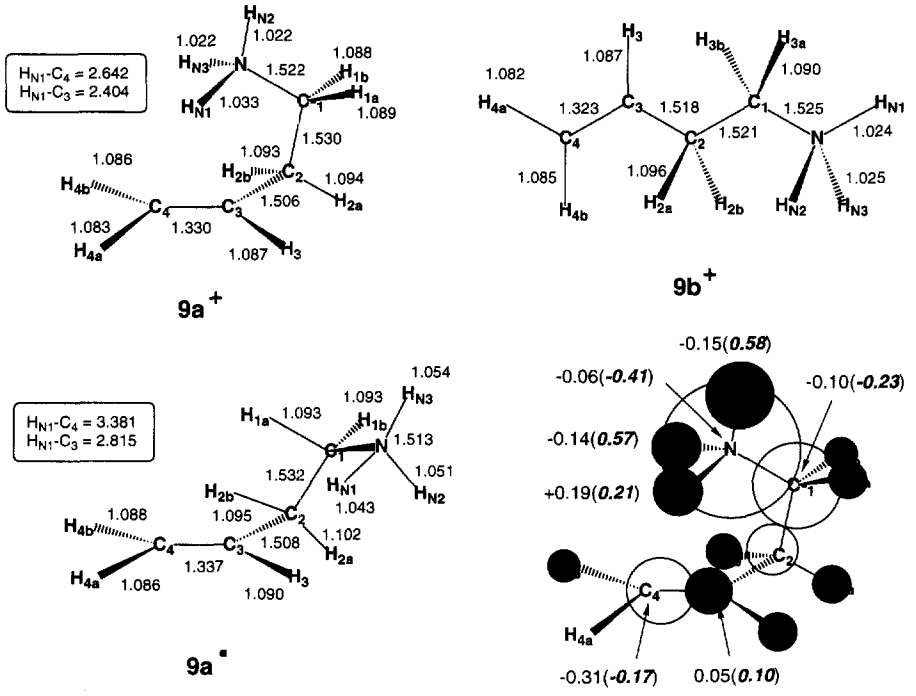

Figure 4. B3LYP/6-311G(2*d*,*p*) optimized structures of **9a**$^+$ and **9b**$^+$ and B3LYP/6-31++G(d,p) optimized structure of **9a**$^•$. Bond lengths in angstroms. SOMO in **9a**$^•$ with total atomic charges (roman) and total atomic spin densities (bold italics).

mized structure of **9a**$^+$ showed somewhat longer C=C and N–H_{N1} bonds due to hydrogen bonding. Similar geometry changes were obtained for **10a**$^+$ and **10b**$^+$, whereby the H-bonded isomer showed slightly longer C=C and O–H_o bonds. The optimized structures also showed that the H-bonded oxonium proton in **10a**$^+$ came closer to the double bond than did the ammonium proton in **9a**$^+$, as documented by the corresponding internuclear C · · · H distances (Figures 4 and 5). The cyclization due to hydrogen bonding also resulted in negative entropy changes, which were relatively greater for **10b**$^+$ and **10a**$^+$ than for **9b**$^+$ and **9b**$^+$ (vide infra) and were consistent with the tighter ring structure in the oxonium ion. The H-bonded ammonium cation **9a**$^+$ was calculated to be more stable than the open-chain isomer **9b**$^+$. However, the calculated enthalpy difference between **9a**$^+$ and **9b**$^+$ was relatively small and did not depend much on the level of theory used (−25 to −28 kJ mol^{-1}, Table 2). It can be concluded that the N–H$^+$ · · · C=C hydrogen bond in **9a**$^+$ is comparable to those in 1,2-amino alcohols and ethers (18–26 kJ mol^{-1} [26, 41]) but weaker than the intramolecular H bonds in 1,3-amino alcohols (40–45 kJ mol^{-1} [42]), or 1,2- and 1,3-diamines (33–41 and 65–67 kJ mol^{-1}, respectively [43–45]). The calculated free energy difference at the typical ion source temperature of 473 K (ΔG°_{473} = −23 and −26 kJ mol^{-1} from the MP2 and B3LYP enthalpies, respectively, ΔS_{473} = −5.9 J mol^{-1} K^{-1}) indicated that 99.7%–99.9% of **9a**$^+$ is present as the H-bonded form at thermal equilibrium in the gas phase.

The intramolecular O–H · · · C=C bond in the 3-

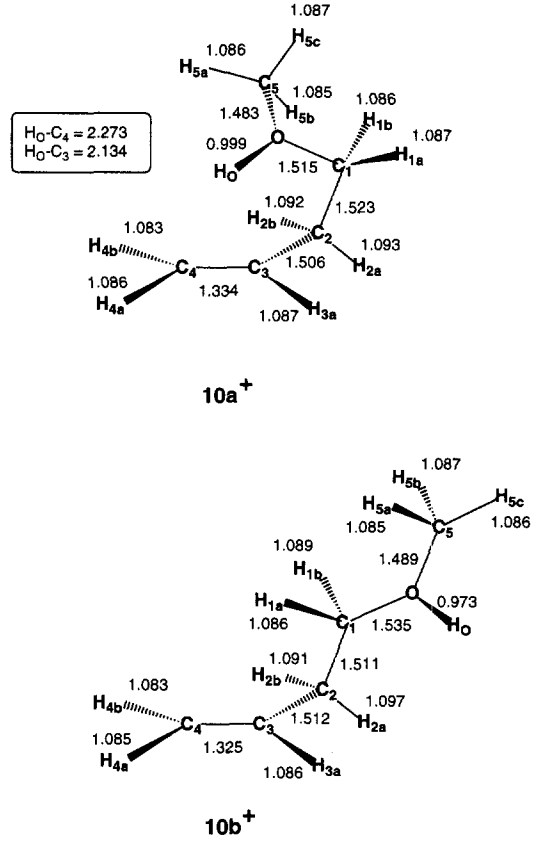

Figure 5. B3LYP/6-311G(2d,p) optimized structures of **10a**$^+$ and **10b**$^+$. Bond lengths in angstroms.

Table 2. Calculated total energies[a]

	RHF/6-31G)(d)	MP2/6-311G(2d,p)	B3LYP/6-311G(2d,p)	B3LYP/6-31++G(d,p)	ZPVE	$H_{298}-H_0$
9a$^+$	−211.499805	−212.362943	−213.003754		357	19.4
9b$^+$	−211.489948	−212.351898	−212.993793		356	20.2
9a$^\bullet$				−213.100637		
9a$^\bullet$(VN)[b]				−213.096165		
10a$^+$	−270.312040		−272.150947		391	23.5
10b$^+$	−270.306947		−272.143643		390	24.5
	B3LYP/6-31(d,p)			B3LYP/6-31++G(d,p)		
11a$^+$	−173.629973					
11a$^\bullet$				−173.787176		
11a$^\bullet$(VN)[b]				−173.785096		

[a] In units of hartree, 1 hartree = 2625.5 kJ mol^{-1}.
[b] Single-point energies on optimized ion geometries corresponding to vertical electron attachment.

buten-1-yl methyloxonium ion favored the cyclic isomer **10a**$^+$ by 18 kJ mol^{-1} as calculated by B3LYP for the 298-K enthalpy difference between **10b**$^+$ and **10a**$^+$ (Table 2). The $\Delta G°_{473}$ for the conversion of **10b**$^+$ to **10a**$^+$ was calculated as −14.5 kJ mol^{-1} (ΔS_{473} = −10.1 J mol^{-1} K^{-1}) favoring the H-bonded isomer. Hence, >97% of the protonated ether should be in the H-bonded form **10a**$^+$ at thermal equilibrium. The equilibrium data calculated for the model 3-buten-1-ylammonium and 3-buten-1-yl methyloxonium cations can be extrapolated readily to the 3-hexen-1-ylammonium and 3-hexen-1-yl methyloxonium ions under study, which should also exist predominantly as H-bonded structures in the gas phase. Likewise, because there are no geometry constraints that would prevent intramolecular H bonding in 4- and 5-hexen-1-ylammonium and oxonium ions, it is reasonable to assume that cations **1**$^+$ and **2**$^+$ and their oxonium analogs [21] existed predominantly as H-bonded structures. In contrast, allylammonium cation **11a**$^+$ was calculated to exist as a single gauche conformer with no intramolecular H bonding to the C=C double bond (Figure 6). A similar gauche conformation was expected for the homologous 2-hexen-1-ylammonium ion **4a**$^+$.

Vertical electron attachment to **9a**$^+$ forms hypervalent radical **9a**$^\bullet$ without changing the ion geometry (Table 2). The geometry relaxation in nascent **9a**$^\bullet$ was investigated computationally. First, the N–C-3 distance was fixed at d(N–C-3) = 3.0 and 3.2 Å, while the other internal degrees of freedom were optimized. These calculations showed an energy decrease by 9 and 12 kJ mol^{-1} at d(N–C-3) = 3.0 and 3.2 Å, respectively, compared with the vertically formed **9a**$^\bullet$. The energy gradient along the N–C-3 coordinate was only 9.2 kJ mol^{-1} Å^{-1} at d(N–C-3) = 3.0 Å. Full optimization gave a local energy minimum corresponding to a gauche conformer **9a**$^\bullet$, which was 12 kJ mol^{-1} lower in energy than the vertically neutralized structure. The main structural differences between **9a**$^+$ and **9a**$^\bullet$ were in the N–H bond lengths, which were longer in the radical, and the torsional angle about the C-1–C-2 bond (Figure 4). In the optimized structure **9a**$^\bullet$ the NH_3 group points away from the double bond, such that there is no N–H · · · C=C hydrogen bond. The long N–H bonds in **9a**$^\bullet$ are in keeping with those computed previously for hypervalent methylammonium radicals [7, 11, 12].

Vertical electron attachment to the allylammonium cation **11**$^+$ forms the hypervalent radical **11a**$^\bullet$. Full optimization of the latter resulted in only a minor geometry relaxation (Figure 6). The Franck–Condon effects upon neutralization, expressed as a difference between the B3LYP/6-31++G(d,p) energies of the vertically formed and relaxed **11a**$^\bullet$, amounted to only 5.4 kJ mol^{-1}.

Although the calculations yielded alkenylammonium radicals **9**$^\bullet$ and **11**$^\bullet$ as local energy minima and indicated small Franck–Condon effects upon vertical electron transfer, the NR experiments showed no survivor ions that would support metastability of hypervalent hexenylammonium radicals on the microsecond time scale. This discrepancy points to the low *kinetic stability* of the

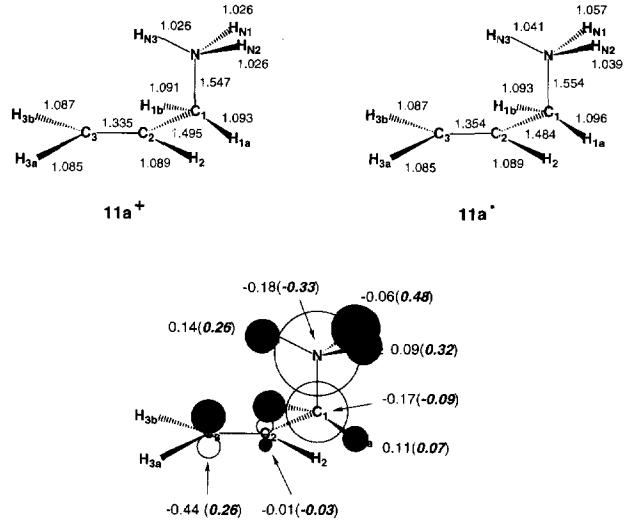

Figure 6. B3LYP/6-31G(d,p) optimized structure of **11a**$^+$ and B3LYP/6-31++G(d,p) optimized structure of **11a**$^\bullet$. Bond lengths in angstroms. SOMO in **11a**$^\bullet$ with total atomic charges (roman) and total atomic spin densities (bold italics).

hypervalent ammonium radicals. By analogy with smaller methylated ammonium radicals for which the dissociation energetics and kinetics are known [7, 10–12], the exothermic dissociation of the N–H bond should require only a small activation barrier (<30 kJ mol^{-1}) in the ground electronic state [7]. The precursor hexenylammonium ions are estimated to have substantial enthalpies, e.g., ~65 kJ mol^{-1} in $\mathbf{5a}^+$ at the ion source temperature of 473 K. The vibrational portion of this thermal energy, ~50 kJ mol^{-1}, goes to the hypervalent radical and is sufficient to drive rapid dissociation by N–H bond cleavage. In addition, excited electronic states can be formed by electron transfer and dissociate by N–C bond cleavage as found for dimethylammonium [12].

The effect on the radical electronic properties of the unpaired electron in $\mathbf{9a}^\bullet$ was investigated by Mulliken population analysis of the UHF/6-31++G(d,p) wavefunction for the vertically reduced structure in its ground (^2A) electronic state. The singly occupied molecular orbital (SOMO) consisted predominantly of diffuse atomic *s* orbitals on C, H, and N (Figure 4). The hydrogen atom which was engaged in H bonding (H_{N1}) carried a positive charge, whereas the negative charge density, typical for hypervalent ammonium radicals, was located at the other two ammonium hydrogen atoms and the backbone carbon atoms. Although the coulombic interaction between the positively charged H_{N1} and the negatively charged C-4 was attractive, the overall multipolar interaction between the negatively charged ammonium group and double bond was repulsive and resulted in a torsional motion about the C-1–C-2 bond, which separated the two moieties and disrupted the hydrogen bond. Rotation about the C-1–C-2 bond to reach the equilibrium geometry showed a continuously negative gradient, which indicated a fast geometry change.

This analysis provides a rationale for the absence of hydrogen transfer in hypervalent alkenylammonium radicals. Following neutralization, the radical undergoes fast relaxation by internal rotation that separates the ammonium groups from the double bond. The energy barrier to N–H bond cleavage is small (cf. 28 kJ mol^{-1} in methylammonium [7]), and comparable to that for H$^\bullet$ atom addition to the double bond (20–35 kJ mol^{-1} [46]). Hence the exothermic dissociation by N–H bond cleavage [7, 11, 12] should outcompete the rearrangement by hydrogen transfer to the double bond.

Population analysis of allylammonium radical $\mathbf{11a}^\bullet$ showed that the SOMO was delocalized over N, C-1, C-3, and the ammonium and methylene hydrogen atoms (Figure 6). The populations were similar in the vertically neutralized and relaxed radical structures. The SOMO consisted mainly of the diffuse 3*s*, 4*s*, and 3*p* atomic orbitals; however, its nodal properties did not resemble those of an atomlike Rydberg orbital. Interestingly and in contrast to methylammonium radicals [7, 11, 12], $\mathbf{11a}^\bullet$ showed substantial negative charge and spin density at the terminal sp^2 carbon atom (C-3, Figure 6). This was due to a through-bond interaction of the π(C=C) orbital with the diffuse (3*s* + 4*s*) σ orbital of the gauche C-1–N bond, which resulted in spin polarization of the 2*p* atomic orbitals at C-3. This analysis showed that the "hypervalence" of the ammonium group depends on the electronic structure of the substituents, and that significant interactions between the ammonium group and substituents exist in larger organic ammonium radicals.

The oxonium radical $\mathbf{10a}^\bullet$ showed an entirely different behavior. In keeping with the previous finding for dimethyloxonium [8], $\mathbf{10a}^\bullet$ was found to be unstable and dissociate without barrier by cleavage of the O–H bond. The latter dissociation showed a substantial negative energy gradient along the O–H coordinate (−104 kJ mol^{-1} $Å^{-1}$) and gained >62 kJ mol^{-1} by stretching the bond from 0.999 Å in the vertically neutralized structure to 1.092 Å in a partially dissociated one. The reaction path for complete dissociation to 1-methoxybut-3-ene and hydrogen atom has not been investigated because of the considerable expense of these calculations. The repulsive potential energy surface along the O–H coordinate indicated a very fast dissociation of $k \approx 10^{14}$ s^{-1}, which should be an order of magnitude faster than the rotation about the C-1–C-2 bond and other intramolecular motions concerning the C-C-C-C-O-C framework. This implies that on the time scale of the O–H bond dissociation, the molecular frame is frozen, and the hydrogen atom is forced to move toward the double bond, where it can be captured to form a C–H bond in a highly exothermic reaction [21]. It should be noted that addition of H$^\bullet$ to the double bond faces a small energy barrier, which can be estimated at 20–35 kJ mol^{-1} [46]. However, this small barrier should be overcome by the substantial energy released by the exothermic dissociation of the O–H bond. In a sense, the exothermic hydrogen transfer in $\mathbf{10a}^\bullet$ can be viewed as an addition of a hot hydrogen atom to an olefin [46].

Hexenyldimethylammonium Ions and Radicals

CID spectra of protonated N, N-dimethylaminohexenes $\mathbf{5a}^+$–$\mathbf{8a}^+$ were studied to identify the neutral fragments formed by ion dissociations. The CID spectra of $\mathbf{5a}^+$–$\mathbf{8a}^+$ differed (Table 3). CID of $\mathbf{5a}^+$–$\mathbf{7a}^+$ showed formations of $C_3H_8N^+$ at *m/z* 58 due to loss of neutral C_5H_{10} and abundant groups of $C_2H_{6-8}N^+$ ions at *m/z* 44–46. Interestingly, the $C_6H_{11}^+$ ion was negligible in $\mathbf{5a}^+$ and $\mathbf{6a}^+$, attesting to an inefficient loss of neutral dimethylamine. The latter dissociation was more prominent in the CID spectra of $\mathbf{7a}^+$ and $\mathbf{8a}^+$ (Table 3). The elimination of dimethylamine from $\mathbf{7a}^+$ and $\mathbf{8a}^+$ is understandable, because it can produce stable homoallylic and allylic hexenyl cations. Deuterium labeling in $\mathbf{5b}^+$ $\mathbf{7b}^+$, and $\mathbf{8b}^+$ showed clean mass shifts for the $C_2H_{6-8}N^+$ ions, which appeared at *m/z* 45–47. This indicated that the neutral fragments, $C_6H_{11}^\bullet$ and C_6H_{10}, respectively, did not retain the ammonium deuterium atom. Moreover, the CID spectra of the deuterium-labeled ions $\mathbf{7b}^+$

Table 3. Collision-induced dissociation spectra of $5a^+$–$8b^+$

	Relative intensity[a]							
m/z	$5a^+$	$5b^+$	$6a^+$	$6b^+$	$7a^+$	$7b^+$	$8a^+$	$8b^+$
18	1	1		0.4	0.3	0.6		0.5
19		2.3		1.2		2.1		1.6
22				2		0.3		
26	0.8	2.4		1.4		2		1.6
27	3.4	15	2.8	11	5.5	16	5.3	14
28	3.5	7	3.2	5.3	5	6	4	5
29	3.8	20	3.8	16	6.5	20	4.3	15
30	2.6	4		3	3.3	3.6		2
31	0.6	6.2		3.6		4		2.8
32		1.6		0.7		1		0.5
33						3.7		0.8
38	0.6	1.5		0.8		1.4		1
39	12	20	8.2	14	11	16	12	12
40	1.7	3.7	1	2.8	2	3.6	2	2.4
41	31	54	16	21	32	49	40	39
42	12	14	10	10	14	15	15	11
43	6	7	5	6	7	8	9	6
44	99	12	54	8.4	83	8.7	100	7.1
45	21	100	29	77	38	98	80	100
46	9	71	18	51	14	64	37	75
47		47		26		21		32
48		1						
50	1	1.5		0.7	1	1.3	1.3	1.7
51	1	1.6		1	1.7	1.8	1	1.3
52	1	1		0.8	1	1.4	1	1
53	6.5	7.3	6.3	6.2	7.7	9.3	9.6	7.2
54	3.3	3.2	2.5	3.2	3.4	4.3	7.7	5.6
55	43	50	57	63	62	73	80	54
56	5.8	5	6.3	6	4	5.6	5.7	4
57	7.2	5.5	6.5	4.4	7	6.6	3.3	2
58	100	97	100	100	100	100	21	12
59	3.8	4.4	3.8	4.5	4.1	3.8	0.8	0.6
60		2.6		1.8		2		1
64						2	1	1.8
65	1	1.7	0.8	2.3	0.7	2.6	1.2	1.5
66						1.2	0.8	1
67	1.6	2	5	4.6	10	10	13	7.7
68	1.2		1.3	1	5.8	5.3	7.3	2
69	1	1.4		1	2.4	3.7	1	3.2
70	14	2.3	4.4	1.3	6.4	1	12	1.3
71	3.4	12	3.2	6.2	1.5	7.6	1	7.8
72	3	1.6	6.6	1.4	0.6	0.8		1.2
73	1	2.8	0.8	6		0.7		
74		1.3		1.3		1		
77	0.8	1		0.6	1	1.3		0.8
79	2.2	2.3	2	1.4	2.7	2.8	3.5	2.2
81	3.5	3.1	3.8	2.5	6.2	6	11	5
82	1.6	1	2.5	2	5.3	3.8	13	5
83	3.7	3.4	2.2	2.7	40	39	88	47
84	17	9	11		4.8	4	17	5.7
85	1.4	3	0.7	3.6	0.7	3	1.6	4
87	2.6	2.2						
96			1.3		2.7		3.1	
97				1.2	0.7	2.4	1.7	1.4
98	1.6		3	1.7	2.6	0.8	5	1.2
99		1		1.8		3	12	1.8
100	0.6					1.4		7
112	4.8		4.7		10		14	
113		4		4.4		9		7
114						1.6		
126	3.4		3.8		4.3		4.1	
127	(13)[b]	2.8	(5)[b]	3.7	(10)[b]	3	(15)[b]	1

(Continued)

Table 3. Collision-induced dissociation spectra of $5a^+$–$8b^+$ *(continued)*

	Relative intensity[a]							
m/z	$5a^+$	$5b^+$	$6a^+$	$6b^+$	$7a^+$	$7b^+$	$8a^+$	$8b^+$
128	–[c]	(15)[b]	–[c]	(28)[b]	–[c]	(15)[b]	–[c]	(13)[b]
129		–[c]		–[c]		–[c]		–[c]

[a] Percent of the most abundant fragment ion.
[b] Relative intensities of ions at *m/z* adjacent to those of the precursors may be affected by artifacts in *B/E* linked scans.
[c] Precursor ion intensities omitted.

and $8b^+$ showed clean losses of $(CH_3)_2ND$, indicating negligible H/D exchange between the dimethylammonium and hexenyl groups. Hence, none of the ion dissociations involved H/D exchange between the dimethylammonium and hexenyl groups.

Neutralization–reionization of $5a^+$–$8a^+$ resulted in complete dissociation of the intermediate radicals $5a^\bullet$–$8a^\bullet$, as no survivor ions were detected in the spectra (Figure 7). The radical dissociations proceeded mainly by N–C bond cleavage to form dimethylamine and $C_6H_{11}^\bullet$. Dimethylamine was detected after reionization as $(CH_3)_2NH^{+\bullet}$ at *m/z* 45 and its fragment ion at *m/z* 44. The [*m/z* 45]/[*m/z* 44] abundance ratios (~0.3) were similar to that in the standard NR mass spectrum of dimethylamine [47]. The energetics of collisional charge transfer in the latter system has been investigated in detail recently; it was estimated that in order to give a ratio of [*m/z* 45]/[*m/z* 44] = 0.3 following collisional reionization, about 65% of $(CH_3)_2NH$ molecules had internal energies in excess of 70 kJ mol^{-1} [47]. By analogy, this implied that the $(CH_3)_2NH$ molecules formed from $5a^\bullet$–$8a^\bullet$ were vibrationally excited such that a large fraction had internal energies exceeding 70 kJ mol^{-1} [47]. The complementary $C_6H_{11}^\bullet$ fragments were not detected as $C_6H_{11}^+$ ions for $5a^\bullet$–$7a^\bullet$ (Figure 7). However, the NR spectra showed their dissociation products at *m/z* 77–83, 67, and 50–55. We did not distinguish whether the dissociations of the hexenyl fragments occurred in the radicals or after collisional ionization, although both neutral and ion dissociations were likely. A $C_6H_{11}^+$ ion was detected in the NR spectrum of $8a^\bullet$ (Figure 7). In this case, a stable allylic ion is expected to be formed by collisional ionization of the 2-hexen-1-yl radical.

Loss of the ammonium hydrogen atom was indicated by the formation of amines **5**–**8** and their dissociations following collisional ionization. For $5^{+\bullet}$–$7^{+\bullet}$, ion fragmentations were dominated (>50% total ion current) by α-cleavage dissociations forming $CH_2{=}N(CH_3)_2^+$ at *m/z* 58 [48]. The ion at *m/z* 58 also appeared as an abundant fragment in the mass spectrum of **8**, which in addition showed fragment ions at *m/z* 98 and 84. The $C_3H_8N^+$ ion thus served as a signature for **5**–**8**. The NR spectra of $5a^+$–$7a^+$ showed the presence of $C_3H_8N^+$ of moderate relative abundance attesting to N–H bond cleavage in the intermediate radicals $5a^\bullet$–$7a^\bullet$. In addition, **5** was indicated by its molecular ion at *m/z* 127 in the NR spectrum of $5a^+$ (Figure 7). In contrast, the *m/z* 127 and 58 ions were of negligible relative intensities in the NR spectrum of $8a^+$, indicating inefficient loss of hydrogen from $8a^\bullet$. Loss of methyl from $5a^\bullet$–$8a^\bullet$ could not be established with certainty because of the lack of signature fragment ions. The potential neutral intermediates, N-methylhexenylamines, were expected to dissociate by α-cleavage following ionization to form $CH_2{=}NHCH_3$ at *m/z* 44 [49], which, however, coin-

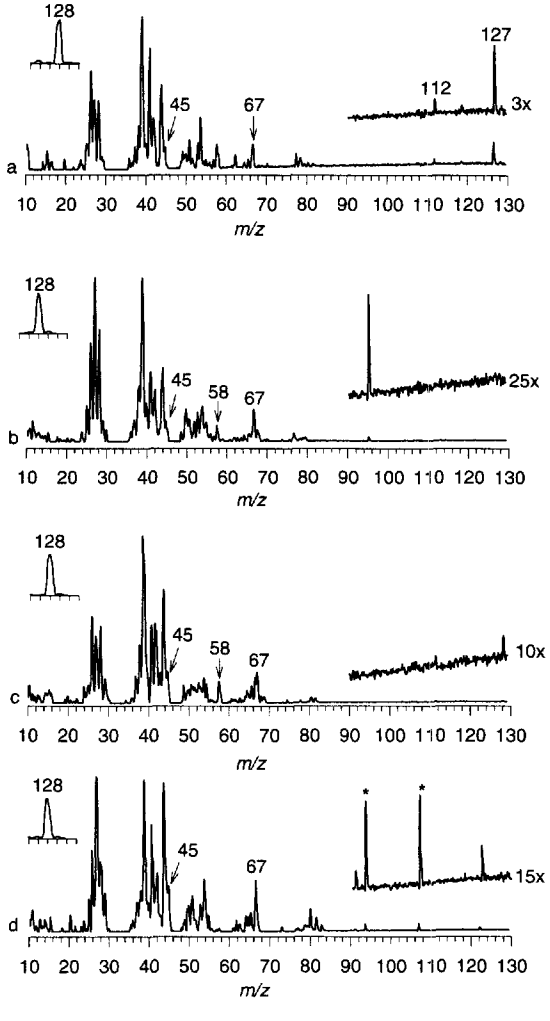

Figure 7. Neutralization–reionization mass spectra of (a) $5a^+$, (b) $6a^+$, (c) $7a^+$, and (d) $8a^+$. The small peaks of *m/z* 94 and 107 in the spectrum of $8a^+$ are probably artifacts. The collision conditions were as in Figure 1. Insets show the $(M + H)^+$ regions in the CI mass spectra.

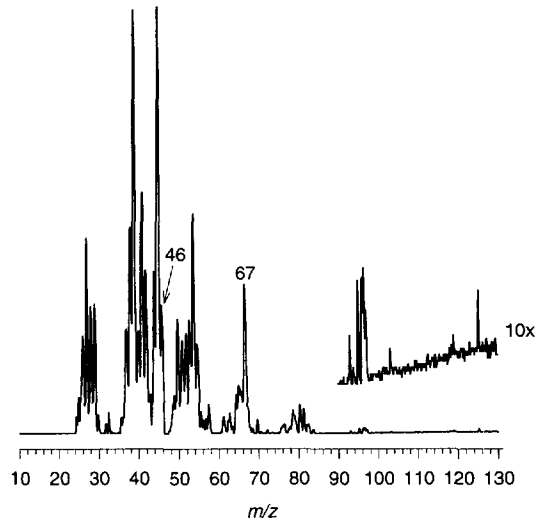

Figure 8. Neutralization–reionization mass spectrum of $\mathbf{8b}^+$. The collision conditions were as in Figure 1.

cided by mass with the fragment from dissociation of dimethylamine. Loss of methyl was weakly indicated by the presence of the fragment at *m/z* 112 in the NR spectrum of $\mathbf{5a}^+$.

Deuterium labeling in $\mathbf{8b}^+$ resulted in mass shifts of the dimethylamine ions, which appeared at *m/z* 45 and 46 (Figure 8). In contrast, no mass shifts due to the presence of deuterium were observed for the hydrocarbon fragments at *m/z* 82, 65–67, 50–55, and 38–42. This implied that intramolecular transfer of the ammonium deuteron did not compete with the bond dissociations.

The results from analysis of the NR spectra of $\mathbf{5a}^+$–$\mathbf{8a}^+$ can be summarized as follows. Hypervalent hexenyldimethylammonium radicals $\mathbf{5a}^{\bullet}$–$\mathbf{8a}^{\bullet}$ were unstable on the 5.4-μs time scale of these measurements. The allylic dimethylammonium radical $\mathbf{8a}^{\bullet}$ dissociated mainly by N–C bond cleavage, whereas losses of $H^{\bullet}$ and $CH_3^{\bullet}$ were less efficient. Radicals $\mathbf{5a}^{\bullet}$–$\mathbf{7a}^{\bullet}$ dissociated by N–C and N–H bond cleavages. The dissociations of $\mathbf{5a}^{\bullet}$–$\mathbf{8a}^{\bullet}$ were similar to those of the saturated N,N-dimethyl-*n*-heptylammonium radical described previously [13].

Conclusions

This combined experimental and computational study of hypervalent organic ammonium radicals allowed us to arrive at the following conclusions. The calculations predicted that primary ammonium radicals were bound, whereas complete dissociation was observed upon neutralization–reionization in the gas phase. The bond dissociation energies in the radicals thus must be low. Competing dissociations by N–H and N–C bond cleavages were observed for radicals in which the double bond was in the remote 3-, 4-, or 5-positions. Hypervalent ammonium radicals of the allylic type showed predominant cleavage of allylic N–C bonds whereas the N–H bond cleavage was less frequent. These dissociations may proceed competitively from the same electronic state. Deuterium labeling showed that there was no hydrogen exchange between the ammonium groups and the hexenyl double bonds. This result was interpreted by DFT calculations, which showed that the interaction between the ammonium group and the double bond was repulsive and prevented hydrogen transfer. The reasons for the preferential N–H bond dissociation as opposed to H transfer are kinetic in nature, because both reactions are exothermic and therefore thermodynamically possible.

DFT analysis also showed that hydrogen transfer was possible in hypervalent radicals derived from unsaturated ethers. The oxonium radicals were unbound with respect to exothermic dissociation of the O–H bond. The repulsive nature of the O···H interaction may provide kinetic energy for the departing hydrogen atom that allows it to overcome a small activation barrier for addition to a suitably positioned C=C double bond. The favorable interaction of the O–H bond and the C=C double bond is secured by hydrogen bonding in the precursor cation, which is preserved in the nascent radical due to the femtosecond time scale of fast collisional transfer.

Acknowledgments

Support of this work by the National Science Foundation (grant no. CHE-9412774) is gratefully acknowledged. The computations were conducted using the resources of the Cornell Theory Center, which received major funding from the National Science Foundation and New York State with additional support from the Advanced Research Projects Agency, the National Center for Research Resources at the National Institutes of Health, IBM Corporation, and members of the Corporate Research Institute. We also thank Dr. Martin Sadilek and Aaron Frank for technical assistance.

References

1. Holmes, J. L. *Mass Spectrom. Rev.* **1989,** *8,* 513.
2. McLafferty, F. W. *Int. J. Mass Spectrom. Ion Processes* **1992,** *118/119,* 221.
3. Tureček, F. *Org. Mass Spectrom.* **1992,** *27,* 1087.
4. Goldberg, N.; Schwarz, H. *Acc. Chem. Res.* **1994,** *27,* 347.
5. Lewis, G. N. *J. Am. Chem. Soc.* **1916,** *38,* 762.
6. Reed, A. E.; Schleyer, P. v. R. *J. Am. Chem. Soc.* **1990,** *112,* 1434.
7. Boldyrev, A. I.; Simons, J. *J. Chem. Phys.* **1992,** *97,* 6621.
8. Sadilek, M.; Turecek, F. *J. Phys. Chem.* **1996,** *100,* 9610.
9. Sadilek, M.; Turecek, F. *J. Phys. Chem.* **1996,** *100,* 15027.
10. Raksit, A. B.; Jeon, S.-J.; Porter, R. F. *J. Phys. Chem.* **1986,** *90,* 2298.
11. Shaffer, S. A.; Tureček, F. *J. Am. Chem. Soc.* **1994,** *116,* 8647.
12. Nguyen, V. Q.; Sadílek, M.; Frank, A. J.; Ferrier, J. G.; Tureček, F. *J. Phys. Chem. A* **1997,** *101,* 3789.
13. Shaffer, S. A.; Tureček, F. *J. Am. Soc. Mass Spectrom.* **1995,** *6,* 1004.
14. Wolken, J. K.; Nguyen, V. Q.; Turecek, F. *J. Mass Spectrom.*, in press.
15. Frøsig, L.; Wolken, J. K.; Tureček, F.; Nguyen, V. Q. *Proceedings of the 44th ASMS Conference on Mass Spectrometry and Allied Topics;* Portland, OR, 1996; p 95.

16. Shaffer, S. A.; Sadílek, M.; Tureček, F. *J. Org. Chem.* **1996,** *61,* 5234.
17. Gellene, G. I.; Porter, R. F. *J. Phys. Chem.* **1984,** *88,* 6680.
18. Kassab, E.; Evleth, E. M. *J. Am. Chem. Soc.* **1987,** *109,* 1653.
19. Boldyrev, A. I.; Simons, J. *J. Phys. Chem.* **1992,** *96,* 8840.
20. Wright, J. S.; McKay, D. *J. Phys. Chem.* **1996,** *100,* 7392.
21. Shaffer, S. A.; Sadilek, M.; Turecek, F.; Hop, C. E. C. A. *Int. J. Mass Spectrom. Ion Processes* **1997,** *160,* 137.
22. (a) Robinson, P. J.; Holbrook, K. A. *Unimolecular Reactions;* Wiley-Interscience: New York, 1972; (b) Gilbert, R. G.; Smith, S. C. *Theory of Unimolecular and Recombination Reactions;* Blackwell: London, 1990.
23. (a) Newcomb, M.; Manek, M. B. *J. Am. Chem. Soc.* **1990,** *112,* 9662. For reviews, see (b) Griller, D.; Ingold, K. U. *Acc. Chem. Res.* **1980,** *13,* 317; (c) Bowman, W. R. In *Organic Reaction Mechanisms,* Knipe, A. C.; Watts, W. E., Eds.; Wiley: Chichester, 1993; Chap. 3, pp 79–116.
24. The relevant proton affinities in kJ mol^{-1} are as follows [25, 26]: ammonia (853), methylamine (901), trimethylamine (942), propene (744), isobutene (802), 2-methyl-2-pentene (828).
25. Szulejko, J. E.; McMahon, T. B. *J. Am. Chem. Soc.* **1993,** *115,* 7839.
26. Lias, S. G.; Liebman, J. F.; Levin, R. D. *J. Phys. Chem. Ref. Data* **1984,** *13,* 695.
27. Parr, R. G.; Yang, W. *Density-Functional Theory of Atoms and Molecules;* Oxford University Press: New York, 1989.
28. Tureček, F.; Gu, M.; Shaffer, S. A. *J. Am. Soc. Mass Spectrom.* **1992,** *3,* 493.
29. Shaffer, S. A. Ph.D. Thesis, University of Washington, 1995.
30. Overman, L. E. *J. Am. Chem. Soc.* **1976,** *98,* 2901.
31. GAUSSIAN 94 (Revision D.1), Frisch, M. J.; Trucks, G. W.; Schlegel, H. B.; Gill, P. M. W.; Johnson, B. G.; Robb, M. A.; Cheeseman, J. R.; Keith, T. A.; Petersson, G. A.; Montgomery, J. A.; Raghavachari, K.; Al-Laham, M. A.; Zakzewski, V. G.; Ortiz, J. V.; Foresman, J. B.; Cioslowski, J.; Stefanov, B. B.; Nanayakkara, A.; Challacombe, M.; Peng, C. Y.; Ayala, P. Y.; Chen, W.; Wong, M. W.; Andres, J. L.; Replogle, E. S.; Gomperts, R.; Martin, R. L.; Fox, D. J.; Binkley, J. S.; Defrees, D. J.; Baker, J.; Stewart, J. P.; Head-Gordon, M.; Gonzalez, C.; Pople, J. A. Gaussian: Pittsburgh, PA, 1995.
32. Hehre, W. J.; Radom, L.; Schleyer, P. v. R.; Pople, J. A. *Ab Initio Molecular Orbital Theory;* Wiley: New York, 1986.
33. Møller, C.; Plesset, M. S. *Phys. Rev.* **1934,** *46,* 618.
34. Pople, J. A.; Head-Gordon, M.; Raghavachari, K. *J. Chem. Phys.* **1987,** *87,* 5968.
35. Hillebrand, C.; Klessinger, M.; Eckert-Maksic, M.; Maksic, Z. B. *J. Phys. Chem.* **1996,** *100,* 9698.
36. Nguyen, V. Q.; Turecek, F. *J. Mass Spectrom.* **1996,** *31,* 1173.
37. Nguyen, V. Q.; Turecek, F. *J. Mass Spectrom.* **1997,** *32,* 55.
38. Nguyen, V. Q.; Turecek, F. *J. Am. Chem. Soc.* **1997,** *119,* 2280.
39. Becke, A. D. *J. Chem. Phys.* **1993,** *98,* 5648.
40. Franke, W.; Schwarz, H.; Wesdemiotis, C. *Z. Naturforsch.* **1981,** *36B,* 1315.
41. Houriet, R.; Rufenacht, H.; Carrupt, R. A.; Vogel, P.; Tichy, M. *J. Am. Chem. Soc.* **1983,** *105,* 3417.
42. Meot-Ner (Mautner), M.; Hamlet, P.; Hunter, E. P.; Field, F. H. *J. Am. Chem. Soc.* **1980,** *102,* 6393.
43. Aue, D. H.; Webb, H. M.; Bowers, M. T. *J. Am. Chem. Soc.* **1973,** *95,* 2699.
44. Meot-Ner (Mautner), M. *J. Am. Chem. Soc.* **1983,** *105,* 4906.
45. Sharma, R. B.; Blades, A. T.; Kebarle, P. *J. Am. Chem. Soc.* **1984,** *106,* 510.
46. Wong, M. W.; Pross, A.; Radom, L. *J. Am. Chem. Soc.* **1993,** *115,* 11050.
47. Nguyen, V. Q.; Turecek, F. *J. Mass Spectrom.* **1996,** *31,* 843.
48. Shaffer, S. A.; Turecek, F.; Cerny, R. L. *J. Am. Chem. Soc.* **1993,** *115,* 12117.
49. McLafferty, F. W.; Turecek, F. *Interpretation of Mass Spectra, 4th ed.;* University Science Books: Mill Valley, CA, 1993.